

Origin of the colossal positive and negative thermal expansion in $\text{Ag}_3[\text{Co}(\text{CN})_6]$: an *ab initio* Density Functional Theory study

Mark Calleja†, Andrew L. Goodwin‡, Martin T. Dove‡||

† Cambridge eScience Centre, Centre for Mathematical Sciences, Wilberforce Road, Cambridge, CB3 0WA, UK

‡ Department of Earth Sciences, University of Cambridge, Downing Street, Cambridge, CB2 3EQ, UK

Abstract. DFT calculations have been used to provide insights into the origin of the colossal positive and negative thermal expansion in $\text{Ag}_3[\text{Co}(\text{CN})_6]$. The results confirm that the positive expansion within the trigonal basal plane and the negative expansion in the orthogonal direction are coupled due to the existence of a network defined by nearly-rigid bonds within the chains of Co–C–N–Ag–N–C–Co linkages. The origin of the colossal values of the coefficients of thermal expansion arise from an extremely shallow energy surface that allows a flexing of the structure with small energy cost. The thermal expansion can be achieved with a modest value of the overall Grüneisen parameter. The energy surface is so shallow that we need to incorporate a small empirical dispersive interaction to give ground-state lattice parameters that match experimental values at low temperature. We compare the results with DFT calculations on two isostructural systems: $\text{H}_3[\text{Co}(\text{CN})_6]$, which is known to have much smaller values of the coefficients of thermal expansion, and $\text{Au}_3[\text{Co}(\text{CN})_6]$, which has not yet been synthesised but which is predicted by our calculations to be another candidate material for showing colossal positive and negative thermal expansion.

PACS numbers: 61.43.Fs, 62.20.Dc, 63.50.+x

1. Introduction

Recently we reported diffraction measurements showing colossal thermal expansion in the network structure of $\text{Ag}_3[\text{Co}(\text{CN})_6]$ [1]. Within that paper we presented data showing a positive linear coefficient of expansion within the basal plane of the trigonal unit cell of $\alpha_1 = +132 \text{ MK}^{-1}$, and a negative coefficient for the orthogonal c axis of $\alpha_3 = -130 \text{ MK}^{-1}$ (1 MK^{-1} is equivalent to $1 \times 10^{-6} \text{ K}^{-1}$). To highlight just how large these values are, we compare values for a number of common materials in table 1. In the recent paper [1] we briefly summarised some of the results from an *ab initio* Density Functional Theory (DFT) study; in the present paper we report the results from this study in more detail, together with an extension to the related materials $\text{H}_3[\text{Co}(\text{CN})_6]$ and $\text{Au}_3[\text{Co}(\text{CN})_6]$.

There are two main issues involved in understanding the thermal expansion of $\text{Ag}_3[\text{Co}(\text{CN})_6]$. First is to understand whether the positive expansion in the trigonal basal plane and the negative expansion in the orthogonal direction have a causal

|| To whom correspondence should be addressed; email mtd10@cam.ac.uk

Table 1. Coefficients of the linear thermal expansion tensor, α_n , for a number of common materials. In none of these examples is the thermal expansion caused in any part by the existence of a phase transition. Units of α are MK^{-1} .

Material	Temperature (K)	α_1	α_2	α_3	references
$\text{Ag}_3\text{Co}(\text{CN})_6$	10–500	132	—	–130	[1]
$d\text{-H}_3\text{Co}(\text{CN})_6$	4–300	14.8	—	–2.4	[2]
ZrW_2O_8	0.4–430	–9.1	—	—	[3, 4]
	430–950	–4.9	—	—	[3, 4]
low cordierite	600–1050	6	5	–0.6	[5]
$\text{Cd}(\text{CN})_2$	150–375	–20.4	—	—	[6]
β -quartz	900	1.9	—	–1.1	[7]
NaCl	293	39.6	—	—	[8]

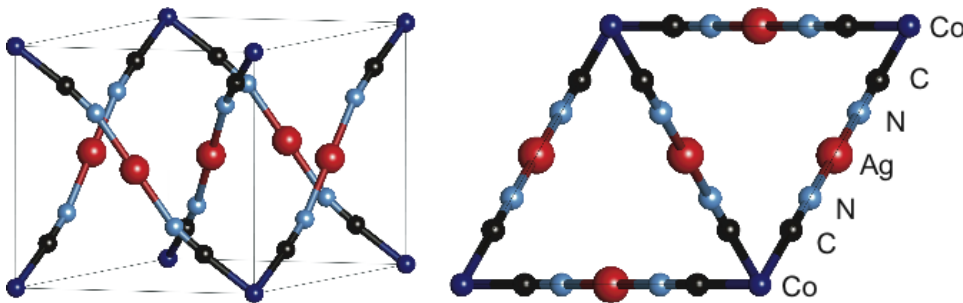


Figure 1. The crystal structure of $\text{Ag}_3[\text{Co}(\text{CN})_6]$, space group $P\bar{3}1m$, showing one unit cell viewed in perspective (left), and as viewed down the crystallographic $[001]$ axis (right). The atoms are labelled in the diagram. We note that the Ag atoms are the large (red) spheres at $z = 1/2$, the Co atoms are the small spheres at the origin of the unit cell (dark blue), the N atoms are the spheres closest to the Ag atoms (light blue), and the C atoms are the spheres closest to the Co atoms (black). Points to note are the existence of CoC_6 octahedra located on the corners of the unit cell, and the Co-C-N-Ag-N-C-Co chains lying across the set of $\{100\}$ planes. Colour is only available in the on-line version.

relationship. An inspection of the crystal structure, figure 1 suggests that the origin of the coupling between the positive and negative expansions lies in the way that the structure forms networks consisting of chains of Co-C-N-Ag-N-C-Co linkages, connecting CoC_6 octahedra via N-Ag-N linear groups. If the $\text{Co}\dots\text{Co}$ chains remain nearly-rigid and nearly-linear, it is an inevitable consequence of the existence of this network of chains that any expansion in the basal plane has to drive a contraction of nearly equal magnitude in the orthogonal direction. However, this fact needs to be quantified. The second issue concerns what features of the material give rise to colossal values of the coefficients of thermal expansion.

Issues such as these are within the domain of atomistic simulation. In the first instance, we judged that empirical models for $\text{Ag}_3[\text{Co}(\text{CN})_6]$ would probably be hard to develop (for reasons that include the paucity of appropriate experimental data for tuning parameters, and the fact that the bonding is not likely to be described by the simple standard functions that would provide the necessary starting point), and thus we have started directly with DFT methods. These are described in the next section, and the main results are described in the subsequent section. We also report a set of calculations for the isostructural material $\text{H}_3[\text{Co}(\text{CN})_6]$, which has the same

coupled positive and negative expansion but with coefficients that are closer to most other materials (table 1), and for $\text{Au}_3[\text{Co}(\text{CN})_6]$, concerning which there are currently no experimental data but which is predicted from our calculations to have similar behaviour to $\text{Ag}_3[\text{Co}(\text{CN})_6]$. The final section reports a simple analysis based on the calculations, showing that the colossal thermal expansion in $\text{Ag}_3[\text{Co}(\text{CN})_6]$ can be accounted for with a modest value of the overall Grüneisen parameter.

We would like to point the reader to a parallel paper that reports the results of a neutron total scattering study of $\text{Ag}_3[\text{Co}(\text{CN})_6]$ [9]. It contains additional discussion of the crystal structure, and presents a number of results that support the work of the present paper.

2. Methods

2.1. DFT calculations

The DFT calculations were performed using the academic version of the CASTEP code, v4.2 [10] operating in energy minimisation mode. This approach uses a plane-wave representation of the electronic basis states, and represents the inner atomic electronic orbitals through the pseudopotential approximation. We used both norm-conserving (NCP) and ultrasoft (USP) pseudopotentials in various calculations, always using the generalised gradient approximation (GGA) to the exchange-correlation energy. The NCP pseudopotentials were generated using the OPIUM code [11], and the USP pseudopotentials were used as supplied with CASTEP with the exception of Co, which was kindly generated for us by Dr Victor Milman (Accelrys). In all our calculations we relaxed the crystal structure to give the lowest energy; this always involved relaxing the atomic coordinates, and in various calculations we either performed a full relaxation of the lattice parameters, or a partial relaxation, or we held the lattice parameters at fixed values.

Anticipating the results we present below, we found that DFT is unable to reproduce the correct ground-state structure of $\text{Ag}_3[\text{Co}(\text{CN})_6]$ for reasons that we subsequently realised point to some scientific insights. Thus we tried a number of approaches, and in this paper we report the calculations on $\text{Ag}_3[\text{Co}(\text{CN})_6]$ using both the NCP and USP models; the calculations on $\text{H}_3[\text{Co}(\text{CN})_6]$ and $\text{Au}_3[\text{Co}(\text{CN})_6]$ were performed using the NCP model only. The plane-wave energy cutoffs used in the NCP and USP calculations were 680 and 470 eV respectively, obtained as good values from convergence tests. As is usual for this type of calculation, the Bloch functions were sampled over a grid of wave vectors using the standard Monkhorst–Pack grid [12], in both cases finding that converged results were obtained using a $3 \times 3 \times 3$ grid.

The trial crystal structure used in each simulation was that determined by Pauling and Pauling [13] for $\text{Ag}_3[\text{Co}(\text{CN})_6]$, as confirmed by our recent neutron diffraction measurements [1]. Where we adjusted lattice parameters (e.g. for running calculations across a grid of pre-set lattice parameters) we used the same set of experimental fractional atomic coordinates for the starting structure. The trial crystal structure had space group $P\bar{3}1m$ (see table 2). There is no automatic method for constraining the crystal symmetry during the energy relaxation process within CASTEP, but the output results showed that the symmetry did not change through any of our relaxation calculations. The simulations on $\text{H}_3[\text{Co}(\text{CN})_6]$ were started with the experimental lattice parameters and fractional atomic coordinates. In the absence of experimental data, the simulations on $\text{Au}_3[\text{Co}(\text{CN})_6]$ used the trial structure of $\text{Ag}_3[\text{Co}(\text{CN})_6]$ as

Table 2. Results for the calculated ground state of $\text{Ag}_3[\text{Co}(\text{CN})_6]$ from the different models using the CASTEP calculations: norm-conserving pseudopotentials (NCP), ultrasoft pseudopotentials (USP), and compared with experimental data for temperatures of 10 K [9] and 300 K [1]. Note that the asymmetric atomic basis is defined with coordinates Co (0,0,0), Ag (1/2,0,1/2), C ($x,0,z$), N (x,o,z), with values for the atomic fractional coordinates x and z given here.

	Experiment (10 K)	Experiment (300 K)	NCP	USP
a (Å)	6.754	7.031	7.764	7.697
c (Å)	7.381	7.117	6.485	6.681
C x	0.222	0.210	0.199	0.198
C z	0.156	0.158	0.174	0.167
N x	0.339	0.335	0.317	0.317
N z	0.264	0.269	0.286	0.278
C–N (Å)	1.122	1.182	1.205	1.179
Ag–N (Å)	2.053	2.012	2.062	2.045
Co–C (Å)	1.890	1.856	1.916	1.889
Ag–Ag (Å)	3.377	3.516	3.882	3.849

the starting point.

2.2. Computational details

The CASTEP jobs were all run on the high-throughput computing grid of the University of Cambridge, CamGrid [14, 15]. This consists of a large number of 4-core (dual processors, with each processor having dual cores, and with 2 GB memory per core) shared-memory machines. Jobs were scheduled using the Condor middleware [16]. Each job was restricted to a single node (one node being a 4-core machine), and run as a 4-processor parallel task. CASTEP was compiled with an Intel F95 compiler (v9.1), and built for the LAM flavour of MPI [17]. By selecting the `coll_shmem` SSI module for LAM, all inter-process communications used shared memory. This avoided the computation making unnecessary use of the network stack, which would have degraded communication speed.

3. Results

3.1. Ground state calculations on $\text{Ag}_3[\text{Co}(\text{CN})_6]$

The results of complete structure-relaxation calculations for both USP and NCP models are presented in table 2. The striking point is that there is a substantial error in the values of the a and c lattice parameters – up to 15% – although the Co–N, Ag–N, and C–N bond lengths are in good agreement with experiment, with errors of around 2% (maximum error is for the Co–C distance in the NCP calculation and is 3.6%). The discrepancies in individual bond lengths are typical for this type of calculation (the community experience is that GGA usually leads to a small over-estimate of bond lengths), but the large errors in calculated lattice parameters are not expected for the methods we used. We believe that the large discrepancy between experiment and calculations is actually providing some critical information about the physics and chemistry of $\text{Ag}_3[\text{Co}(\text{CN})_6]$, suggesting that an important feature is missing from the DFT calculations. Anticipating results described later in this paper, we note that our calculations on $\text{H}_3[\text{Co}(\text{CN})_6]$ gave results that are much closer to experiments (within

Table 3. Mulliken atomic charges (Q) and Mulliken bond orders (BO) calculated for $\text{Ag}_3[\text{Co}(\text{CN})_6]$ (first four columns of data) and $\text{H}_3[\text{Co}(\text{CN})_6]$ and $\text{Au}_3[\text{Co}(\text{CN})_6]$ (last two columns). NCP and USP correspond to the use of norm-conserving pseudopotentials and ultrasoft pseudopotentials respectively, and MIN and EXP refer to the lattice parameters of $\text{Ag}_3[\text{Co}(\text{CN})_6]$ after minimisation and with the experimental values respectively.

	NCP_MIN	USP_MIN	NCP_EXP	USP_EXP	$\text{H}_3[\text{Co}(\text{CN})_6]$	$\text{Au}_3[\text{Co}(\text{CN})_6]$
Q_{Co}	1.13	1.15	1.16	1.19	1.32	1.18
$Q_{\text{Ag/H/Au}}$	0.68	0.61	0.65	0.58	0.36	0.54
Q_{C}	-0.01	-0.02	-0.01	-0.02	0.05	0.00
Q_{N}	-0.52	-0.48	-0.51	-0.47	-0.45	-0.47
BO Co-C	0.25	0.20	0.25	0.19	0.22	0.25
BO C-N	1.80	1.84	1.80	1.84	1.77	1.81
BO Ag/H/Au-N	0.33	0.35	0.34	0.37	0.43	0.41
BO Ag-Ag/H-H/Au-Au	-0.01	-0.03	0.00	-0.02	0.00	0.00

the usual GGA level of agreement), suggesting that the discrepancies are due to some specific feature of the Ag cations.

Given that the DFT calculations are giving reasonable results for the individual bond lengths, we repeated the calculations in which the lattice parameters are held at their experimental values and atomic coordinates were allowed to relax. For the NCP and USP models, the energy differences are 0.111 and 0.169 eV per formula unit respectively (0.037 and 0.056 eV per Ag atom respectively). This is actually quite a small difference, and suggests that whatever is missing from the DFT calculations is not large, but nevertheless appears to be significant in the present case because overall energy differences are small. It is also interesting to note that the DFT results do not show any appreciable rearrangement of the atomic charges or change in the bonding characteristics when changing the lattice parameters — the calculated Mulliken charge distribution and Mulliken bond orders obtained directly from the CASTEP calculations [18, 19] are given in table 3, and show no significant changes with large changes in lattice parameters.

Our hypothesis is that the large discrepancies between the experiment and calculated ground state structures can be traced to the Ag...Ag nearest-neighbour (non-bonded) distance, which is half the value of the a lattice parameter. This is longer in the calculation than experiment by 0.5 Å. The Ag...Ag distance at low temperature – 3.38 Å – is of the same size as twice the Van der Waal’s radius (1.72 Å), and thus might be considered to be rather short in view of the fact that this is a charged cation (DFT charge value is of order 0.6 positive electron units). The electron density obtained from the NCP calculations is presented in figure 2. This shows that there is no covalent bonding between the neighbouring Ag cations, although covalent bonding is seen along the Co-C-N-Ag chains. Thus we believe that the expansion in the basal plane in the calculation relative to the experimental structure can be understood as arising from a repulsion between the neighbouring Ag atoms, or equivalently, due to the lack of an additional attractive interaction in the model. In short, there is some aspect of the Ag...Ag interactions that is not properly reflected in the DFT calculations, albeit one that will not give large changes in energy (recall the comparison between the calculations with complete structure relaxation and those held at the experimental lattice parameters above).

At this point we note the work of Pyykkö and co-workers on metallophilic

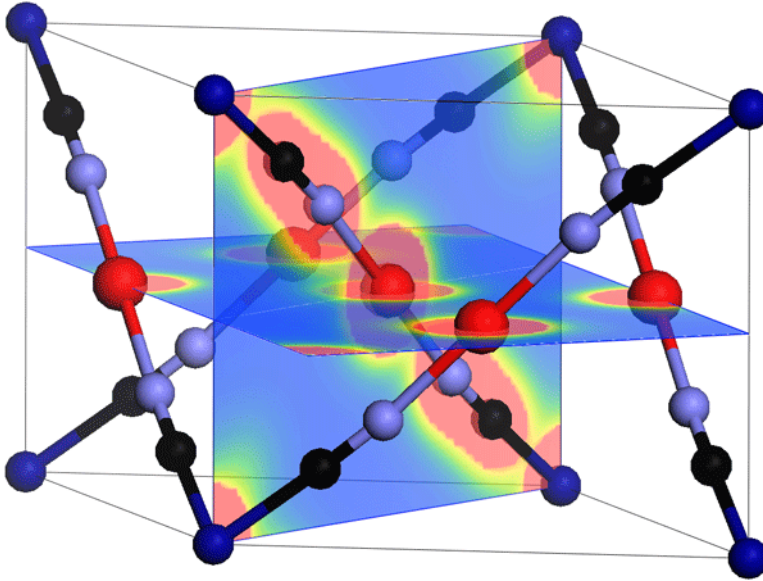


Figure 2. Electron density contour plots for two planes in the crystal structure of $\text{Ag}_3[\text{Co}(\text{CN})_6]$. The vertical plane $(1\bar{1}0)$ contains the Co–C–N–Ag linkages and shows the strong covalent bonding within the C–N group and additional covalent Co–C and Ag–N bonds as electron density between the bonded atoms. The horizontal plane $((001)$ plane at $z = 1/2$) contains the nearest-neighbour Ag cations, and shows no electron density between these atoms. The labelling of the atoms is as given in figure 1. Colour is only available in the on-line version.

interactions involving group 11 elements [20, 21, 22]. These appear to arise due to electron correlation effects that are not included within the DFT approach [23], and can be represented as an enhanced dispersive interaction. Based on this, we have attempted to correct for the discrepancies between calculation and experiment in $\text{Ag}_3[\text{Co}(\text{CN})_6]$ by adding a *post hoc* dispersive interaction between the Ag atoms of the form $-Cr^{-6}$. We find that the minimum energy state with lattice parameters closest to the experimental low-temperature values can be achieved using a value of C of $80 \text{ eV } \text{\AA}^6$ per atom pair. We should remark that in general *post hoc* corrections would not be expected to give consistent results, because we minimise the atomic coordinates without the correction. However, in the present case the calculations show that the bond lengths remain more-or-less constant independent of the values of the a and c lattice parameters, and thus we do not expect the inclusion of the *post hoc* correction to significantly affect bond lengths. Of course, we could have also included dispersive interactions involving the C and N atoms, but based on our calculations of $\text{H}_3[\text{Co}(\text{CN})_6]$ presented below we have compelling evidence that the Ag...Ag interactions are the critical ones here. In any case we anticipate that any effects of the C and N atoms will be incorporated into the Ag...Ag interaction we included through the value of C we used. Thus we conclude that Ag...Ag interactions that are not captured within the DFT method are required to obtain the correct ground state of $\text{Ag}_3[\text{Co}(\text{CN})_6]$. However, these are not large and are only noticeable because of the high degree of flexibility of the network that defines the crystal structure. We show below that this additional interaction actually softens the energy

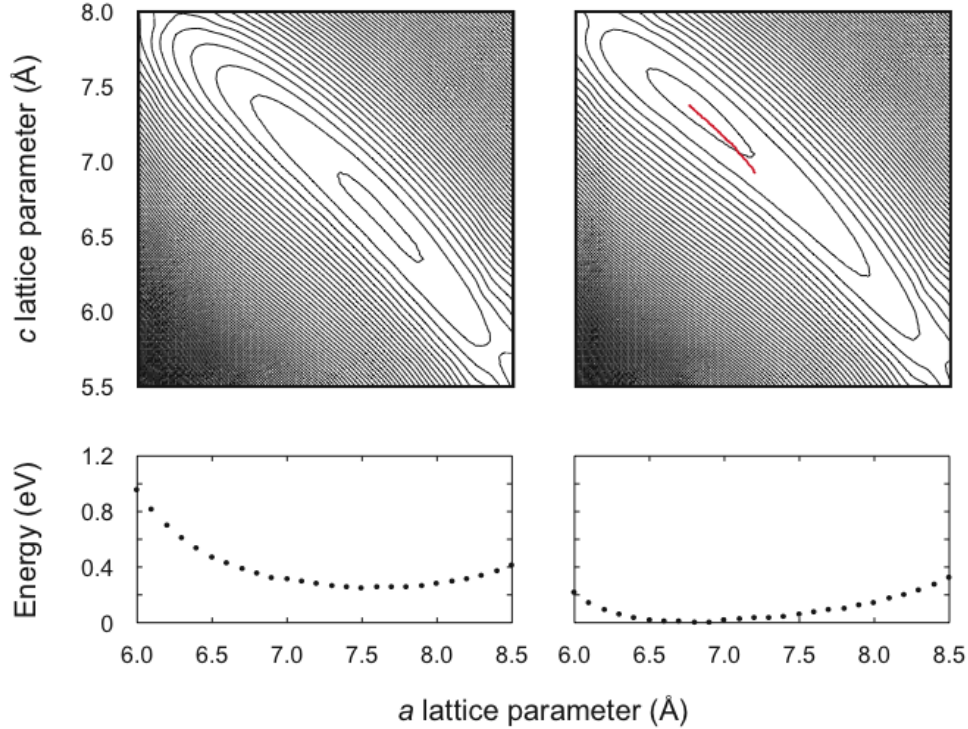


Figure 3. Contour plots for the grid of calculations for $\text{Ag}_3[\text{Co}(\text{CN})_6]$ holding a and c at fixed values, obtained using with norm-conserving pseudopotentials without (*top left*) and with (*top right*) the *post hoc* dispersive interaction. The line of points (red in on-line version) show the locus of experimental data. The lower curves trace the energy of the locus of points along the bottom of the valley in the contour plots.

surface, and is implicated in the ability of this material to show colossal positive and negative thermal expansion.

3.2. Energy surface for $\text{Ag}_3[\text{Co}(\text{CN})_6]$

In figure 3 we plot the energy surface computed for a grid of fixed values of a and c for the model with norm-conserving pseudopotentials, allowing relaxation of the atomic coordinates for each calculation. The results are shown with and without the *post hoc* dispersive interaction. The key result is that the energy surface consists of a very steep valley with an extremely shallow ‘floor’. The *post hoc* additional dispersive interaction has little effect on the overall shape of the valley, but shifts the minimum point along the floor. Figure 3 also contains the locus of experimental data for a and c for various temperatures [1]; the position of this locus is very close to the calculated valley floor, confirming that the DFT calculations are capturing the correlation between the values of a and c seen in experiment. In figure 3 we also plot the energy from from the locus of minima points obtained by holding fixed values of a and b and allowing c to relax.

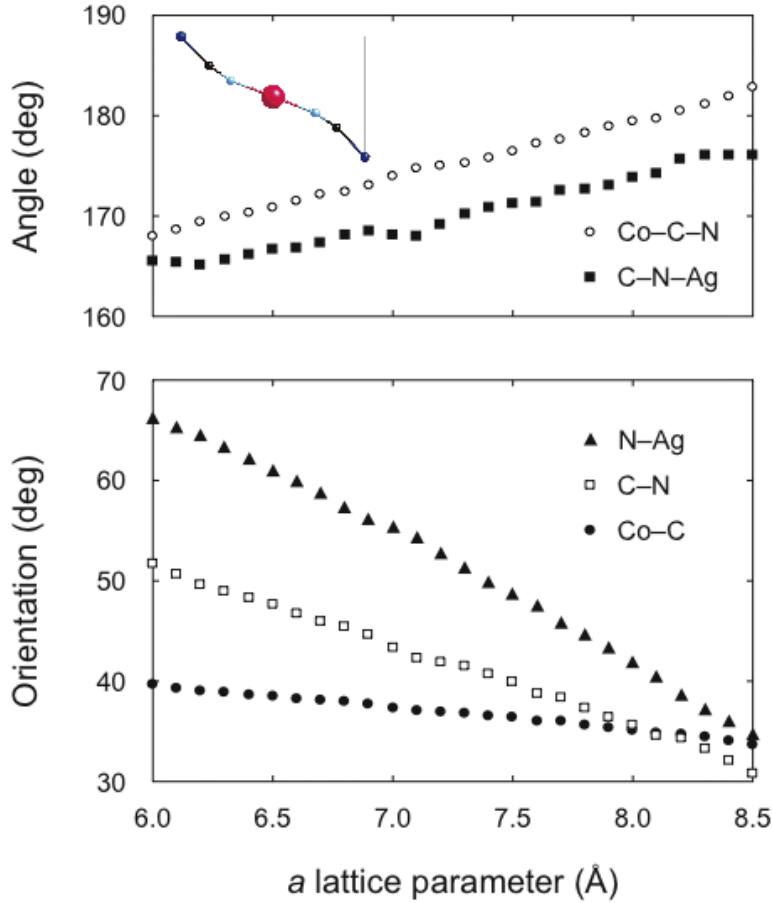


Figure 4. Plots of the angles (*top*) and orientations with respect to the (001) plane (*bottom*) of the nearest-neighbour bonds in $\text{Ag}_3[\text{Co}(\text{CN})_6]$, calculated using fixed values of a and allowing c and the atomic coordinates to relax. The angles are defined such that the angles in the cartoon, which corresponds to the structure for $a = 6.0$ Å, are both acute, and the orientations are given with respect to the horizontal line (see cartoon).

3.3. Structure analysis

We note here that the Co-N, C-N and N-Ag bond lengths do not change significantly across the range of the calculations. Maximum changes in bond lengths for the Co-N and N-Ag bonds are 1% and 0.8% respectively for the range of calculations in which we held the a lattice parameter fixed at values between 6 and 8.5 Å, and allowed relaxation of the c lattice parameter and of the atomic coordinates. The change in the C-N bond length across the range of calculations is even smaller, 0.1%.

Thus the largest changes in the structure for large changes in the lattice parameters are in the orientations of the bonds, or equivalently in the bond angles. In figure 4 we plot the calculated Co-C-N and C-N-Ag bond angles (*top*), and the calculated orientations of the Co-C, C-N and N-Ag bonds with respect to the (001) plane (*bottom*), all as a function of the lattice parameter a obtained with relaxation of

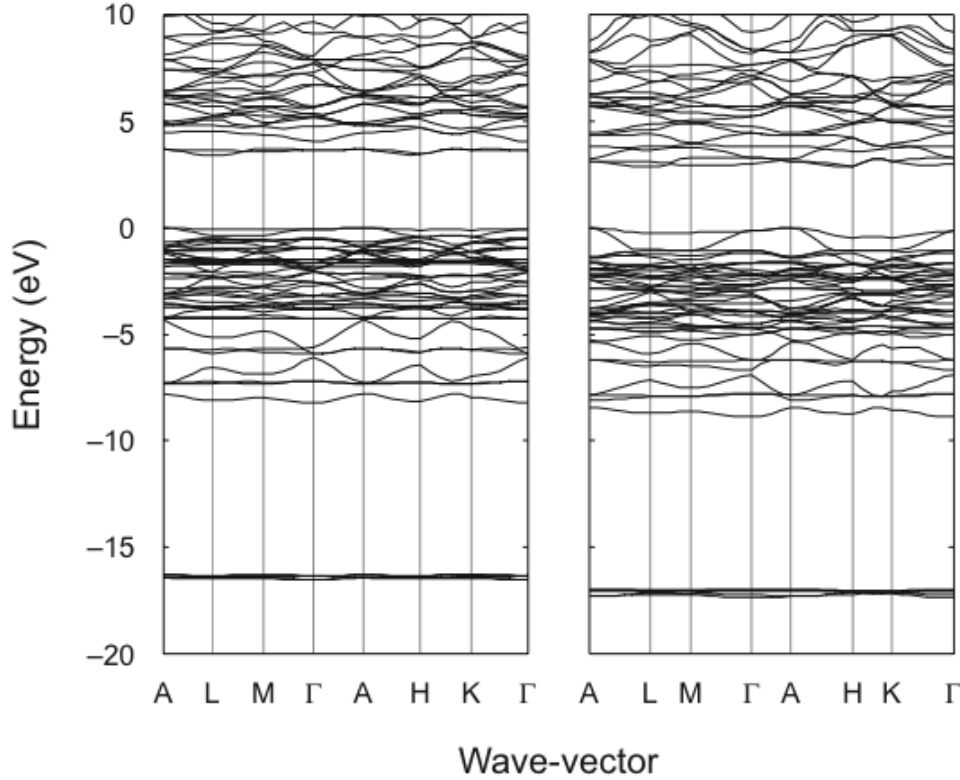


Figure 5. Plots of the DFT band structure of $\text{Ag}_3[\text{Co}(\text{CN})_6]$ computed at the values of lattice parameter $a = 7.7652 \text{ \AA}$ of the minimum DFT energy structure (*left*) and for $a = 6.0 \text{ \AA}$ (*right*; lattice parameter c and atomic coordinates were at relaxed values).

c and the atomic coordinates. Note that a linear Co–C–N–Ag chain will correspond to the three orientations being equal. Thus we note that for large values of the a lattice parameter we have a greater tendency towards forming linear chains, but on decreasing the value of a we see significant crumpling of these chains. The orientation of the Co–C bond is actually determined by the shape of the CoC_6 octahedron, and the fact that this changes the least – by no more than 5° – is consistent with the fact that the CoC_6 octahedra retain their basic shape across the range of calculations. The C–Co–C angle (not shown in figure 4) varies in a more-or-less linear manner from 84° at $a = 6 \text{ \AA}$ to 92° at $a = 8.5 \text{ \AA}$. In order to accommodate the large decrease in the value of a , and the concomitant increase in the value of c , it is essential that the chain be aligned closer towards the vertical direction. Thus there is a clear need for the chain to buckle, as seen in figure 4. It is interesting to note that the two chain bond angles change by similar amounts (figure 4 *top*), so that the N–Ag bond changes its orientation by the greatest amount (figure 4 *bottom*), rather than the buckling being accommodated more by bending of one bond angle than the other (note that the N–Ag–N linkage is constrained to be linear).

3.4. DFT Band structure

The DFT band structure of $\text{Ag}_3[\text{Co}(\text{CN})_6]$ is shown in figure 5 for two different values of lattice parameter a , namely 6.0 Å and 7.7652 Å (the lattice parameter of the DFT minimum energy structure), computed on structures for which the lattice parameter c and the atomic coordinates had been relaxed. Two points should be noted from the data. First, the DFT band gap – the existence of which is consistent with the experimental observation that $\text{Ag}_3[\text{Co}(\text{CN})_6]$ is an insulator – increased from 2.84 eV to 3.37 eV on increasing a from 6.0 Å to the value of the DFT energy minimum structure. The band gap increases further to 3.70 eV on increasing a to 8.4 Å. Although DFT is known to significantly underestimate the true band gap, trends in the behaviour of the band gap may be considered to be qualitatively reliable. Thus, whilst the changes in the DFT band gap are not large, there is nevertheless an appreciable lowering of the band gap as the Ag atoms come closer together, and as the C...C chains become more vertically inclined. The second point to note is that the splitting of the top two valence bands increases significantly on decreasing a , with one band developing a greater variation with wave vector. These two bands are degenerate at the Γ and A ($\mathbf{k} = 0, 0, 1/2$) points (and along the Γ -A line), and there is maximum splitting along the L-M and H-K lines (L, M and H are $\mathbf{k} = 1/2, 0, 0, 1/2, 0, 0$ and $1/3, 1/3, 1/2$ respectively [24]).

3.5. Aside: orientation of the CN molecular ion

From a purely electrostatic viewpoint, the Co cations might be expected to have N rather than C as its neighbouring atom, particularly as the N component of the CN^- molecular ion contains most of the charge (as seen in table 3). Indeed, all known structural analogues, such as $\text{La}[\text{Ag}(\text{CN})_2]_3$ and $\text{KCo}[\text{Ag}(\text{CN})_2]_3$, have the CN molecular ion rotated by 180° relative to $\text{Ag}_3[\text{Co}(\text{CN})_6]$. This raises the question of whether the orientation of the CN molecular ion in $\text{Ag}_3[\text{Co}(\text{CN})_6]$ is in a genuine equilibrium arrangement, or whether this structure is the metastable result of the growth process. We therefore calculated the energy for the case where we swapped the positions of the C and N atoms, giving Co-N-C-Ag-C-N-Co chains instead of the Co-C-N-Ag-N-C-Co chains found in the experimental structure. Our calculations showed that the experimental structure has the lower energy difference, with an energy difference of 1.03 eV per unit cell from the DFT calculations with the norm-conserving pseudopotentials.

3.6. Calculations on $\text{H}_3[\text{Co}(\text{CN})_6]$

To provide a comparison, we have performed calculations (using the NCP model) on the isostructural material $\text{H}_3[\text{Co}(\text{CN})_6]$. This is a useful comparison because experimental data for $\text{H}_3[\text{Co}(\text{CN})_6]$ show that the thermal expansion is much smaller in this material (see table 1). We used the same structure as for $\text{Ag}_3[\text{Co}(\text{CN})_6]$, with the H lying exactly half way between the neighbouring N atoms. There has been some discussion in the literature concerning whether the positions of the H atoms might be disordered. In particular, the structure reported by Haser *et al* [25] has two sites for each H atom. However, our own recent neutron powder diffraction studies [2] have found no evidence for positional site disorder, with the best structure refinements having the H atoms in ordered positions, albeit with evidence for transverse vibrations as might be expected.

Table 4. Results for the calculated ground state of $\text{H}_3[\text{Co}(\text{CN})_6]$ and $\text{Au}_3[\text{Co}(\text{CN})_6]$; atomic coordinates follow the definition in table 2 with H and Au replacing Ag, and experimental results for deuterated- $\text{H}_3[\text{Co}(\text{CN})_6]$ were obtained at a temperature of 8 K [2].

	$d\text{-H}_3[\text{Co}(\text{CN})_6]$ experiment	$\text{H}_3[\text{Co}(\text{CN})_6]$ calculation	$\text{Au}_3[\text{Co}(\text{CN})_6]$ calculation
a (Å)	6.412	6.545	7.990
c (Å)	5.718	5.678	6.193
C x	0.238	0.238	0.196
C z	0.194	0.198	0.180
N x	0.376	0.377	0.312
N z	0.322	0.324	0.292
C–N	1.151	1.161	1.163
H/Au–N	1.291	1.283	1.978
Co–C	1.885	1.917	1.918
H–H/Au–Au	3.206	3.272	3.995

The results of the DFT calculations are summarised in table 4. The agreement between the structures calculated by DFT and obtained from experiment is reasonable, and in line with the accuracy that is typical for DFT calculations: the errors on the values of a and c are +2% and -0.6% . In light of the above discussion on the role of Ag...Ag interactions, it is interesting to note this good agreement, which indirectly confirms the important role of Ag...Ag interactions in determining the ground state of $\text{Ag}_3[\text{Co}(\text{CN})_6]$.

In figure 6 (left side) we show the contour plot for $\text{H}_3[\text{Co}(\text{CN})_6]$ analogous to the plot shown for $\text{Ag}_3[\text{Co}(\text{CN})_6]$ in figure 3, together with the locus of the minima points along the valley in the energy surface. In comparison with $\text{Ag}_3[\text{Co}(\text{CN})_6]$ we see a similar steep valley in the energy surface that provides the correlation between inverse changes in lattice parameters a and c . However, the changes in energy along the floor of the valley are significantly larger than in $\text{Ag}_3[\text{Co}(\text{CN})_6]$. Given that this is the most significant difference between the calculations for the two materials, we surmise that it is closely associated with the differences in values of the coefficients of thermal expansion.

3.7. Calculations on $\text{Au}_3[\text{Co}(\text{CN})_6]$

Finally, we also report calculations of the ground-state structure of $\text{Au}_3[\text{Co}(\text{CN})_6]$, table 4, and a calculation of the energy surface is shown in figure 6. We believe that $\text{Au}_3[\text{Co}(\text{CN})_6]$ has yet to be synthesised, so these results are predictive. The energy surface is very similar to that of $\text{Ag}_3[\text{Co}(\text{CN})_6]$ (figure 3), and thus we can predict that the thermal expansion will also show a similar correlation between a and c . Moreover, the variation of energy along the floor of the valley in the energy surface is very close in size to that of $\text{Ag}_3[\text{Co}(\text{CN})_6]$ – and is much smaller than that of $\text{H}_3[\text{Co}(\text{CN})_6]$ – so we anticipate that $\text{Au}_3[\text{Co}(\text{CN})_6]$ will have large values of its coefficients of thermal expansion similar in size to those of $\text{Ag}_3[\text{Co}(\text{CN})_6]$. Because there are no experimental data on this structure, it is impossible to judge the extent to which an additional dispersive Au...Au interaction is required to give a complete description of the energy surface, but the work of Pyykkö and co-workers [20, 21, 22] suggest that there should be significant metallophilic interactions as in $\text{Ag}_3[\text{Co}(\text{CN})_6]$. Furthermore, the calculated value of the a lattice parameter is much larger (of order 1.43 Å) than the experimental value

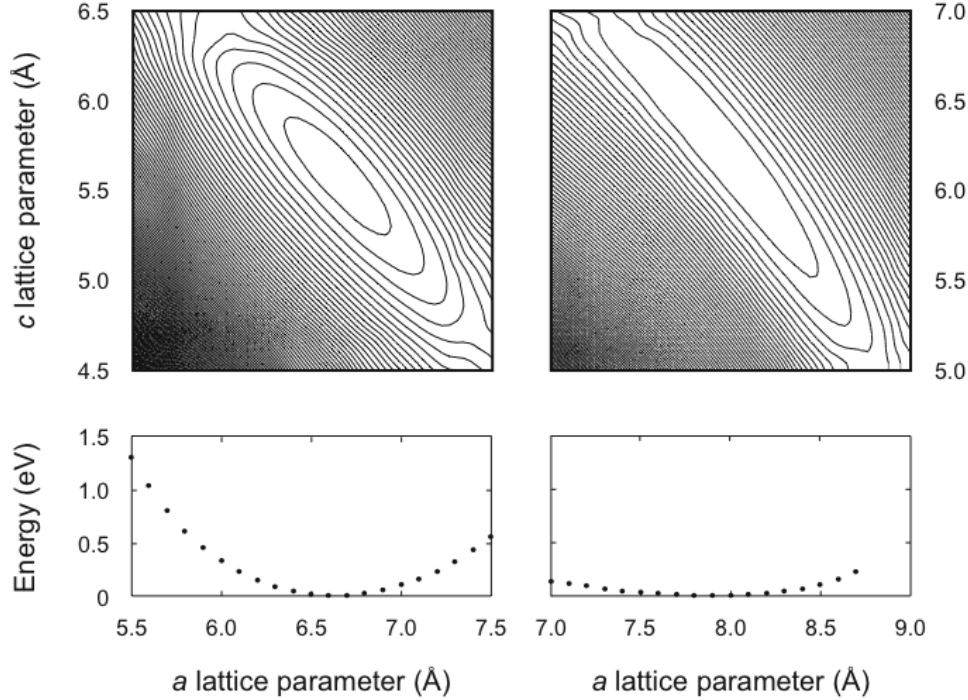


Figure 6. Contour plot for the DFT calculations for $\text{H}_3[\text{Co}(\text{CN})_6]$ (*top left*) and $\text{Au}_3[\text{Co}(\text{CN})_6]$ (*top right*) with the trace of the energy of the locus of points along the bottom of the valley in the contour plot (*bottom*). It is interesting to compare these plots with the data presented in figure 3.

for the isostructural $\text{La}[\text{Au}(\text{CN})_2]_3$, where $a = 6.664 \text{ \AA}$ at 213 K [26]. This suggests that it is highly likely that the behaviour of $\text{Au}_3[\text{Co}(\text{CN})_6]$ and analogues such as $\text{La}[\text{Au}(\text{CN})_2]_3$ will show colossal positive and negative thermal expansion.

4. Analysis

The DFT results shown in figure 3 point clearly to the existence of an energy surface in the space defined by the a and c lattice parameters that consists of a valley with very steep sides but only a shallow slope along the locus of minima points. The shape of the energy surface thus explains the origin of the negative thermal expansion along c for a positive expansion along a , consistent with the intuition from the structure outlined in the Introduction.

We now consider the question of why the coefficients of thermal expansion of $\text{Ag}_3[\text{Co}(\text{CN})_6]$ have colossal magnitudes. In our analysis we anticipate that the thermal expansion can be driven as a normal anharmonic phonon process with a very shallow energy surface. We write the free energy in standard form [27] as

$$F = 3Nk_{\text{B}}T \ln \left(\frac{\hbar\omega}{k_{\text{B}}T} \right) + \frac{1}{2} \frac{\partial^2 E}{\partial V^2} (V - V_0)^2 \quad (1)$$

where V is the volume occupied by N atoms, V_0 is the corresponding volume at the minimum-energy configuration, E is the potential energy of N atoms, and the phonon

free energy has been expressed in the high-temperature limit ($k_{\text{B}}T > \hbar\omega$) where ω represents an average phonon angular frequency. Minimisation with respect to volume yields

$$V = V_0 + 3N\gamma Bk_{\text{B}}T = V_0(1 + \beta T) \quad (2)$$

where γ is the normal overall Grüneisen parameter, and the bulk modulus $B = (V_0\partial^2 E/\partial V^2)^{-1}$. The equation defines $\beta = 3NBk_{\text{B}}\gamma/V_0$. Our approach here is to use the energy calculations and experimental data for β (obtained as the trace of the linear thermal expansion coefficients) to obtain a value for $B\gamma$, and from an estimate for B (this can only be an estimate because of the use of the *post hoc* correction for the dispersive energy) to obtain an estimate of γ . Thus we obtain $B\gamma = 47.3 \times 10^{-12} \text{ Pa}^{-1}$ from the experimental data. The origin of the colossal values of the coefficients of thermal expansion can be expressed in terms of whether $\text{Ag}_3[\text{Co}(\text{CN})_6]$ has an unusually large value of B or γ or both.

From the energy calculations we obtained a fitted value for $B^{-1} = 9.9 \text{ GPa}$, which would yield a value of $\gamma = 0.47$. We stress that our fitted value of B^{-1} is hard to estimate accurately from our DFT data because, being a small value, it is affected by very small errors in the calculations. However, it is nevertheless clear that the value for B^{-1} is small (by comparison, values of B^{-1} for NaCl, CaF_2 and cordierite are 24.4, 82.7 and 129 GPa respectively), so that B is large, and this had been anticipated from the significant strain broadening seen in diffraction experiments [1]. In fact, the value of B is so large that we have obtained a fairly typical estimate (in fact, on the low side of normal) for the value of γ rather than a particularly large value.

We note that we do not anticipate a large value for γ for two reasons: first, because we do not anticipate the bond-stretching vibrational frequencies to change significantly with volume given that the bond lengths and bond orders do not change in the DFT calculation; and second, because negative contributions to the overall Grüneisen parameter will also decrease its value. These will arise from dynamic bond-bending motions along the Co–C–N–Ag–N–C–Co chains, which will have the effect of pulling the end Co atoms closer together.¶ We note that these motions have been observed in our RMC study. The final value of γ will be a balance between motions that expand the volume and those that want to pull the structure inwards.

What this analysis shows is that the colossal values of the coefficients of thermal expansion can be explained reasonably well with a normal, albeit slightly small, value of the phonon Grüneisen parameter, and that the values of the coefficients of thermal expansion are so large because of the incredibly shallow energy surface along the bottom of the valley.

We repeat this analysis for our results for $\text{H}_3[\text{Co}(\text{CN})_6]$. We obtain $B\gamma = 8.36 \times 10^{-12} \text{ Pa}^{-1}$ from experimental data. Our calculated energy surface gives $B^{-1} = 56.4 \text{ GPa}$, from which we obtain $\gamma = 0.47$. This value of γ is very similar to that of $\text{Ag}_3[\text{Co}(\text{CN})_6]$. The principle difference between the thermal expansion of the two materials is thus due entirely to the different values of B , which is seen in the differences between the energy surfaces.

¶ An analysis of the numbers of structural constraints and degrees of freedom shows that there are 15 more degrees of freedom than constraints per formula unit. This imbalance gives rise to rotational motions of stiff CoC_6 , CN and AgN_2 units that will cause a shortening of the Co...Co chain. These motions correspond to the Rigid Unit Modes that are known to give negative contributions to the overall Grüneisen parameter [6, 28, 29, 30].

Finally, from the shapes of the energy surfaces, and from the result that both $\text{Ag}_3[\text{Co}(\text{CN})_6]$ and $\text{H}_3[\text{Co}(\text{CN})_6]$ have normal values for γ , we make the prediction that $\text{Au}_3[\text{Co}(\text{CN})_6]$ will also show the same behaviour for its thermal expansion as $\text{Ag}_3[\text{Co}(\text{CN})_6]$, as also may other isostructural materials containing silver or gold. The main challenge involved in studying this compound experimentally is the limited aqueous chemistry of the Au^+ cation, which prevents a simple modification of the synthetic route for $\text{Ag}_3[\text{Co}(\text{CN})_6]$.

5. Conclusion

In this paper we have used DFT calculations to demonstrate that the coupled positive and negative thermal expansion in $\text{Ag}_3[\text{Co}(\text{CN})_6]$ and $\text{H}_3[\text{Co}(\text{CN})_6]$ arises from the existence of steep valley in the appropriate energy surface that can be traced to the existence of chains of atoms within the crystal structure that can flex like a garden trellis. The floor of the valley is particularly shallow in the case of $\text{Ag}_3[\text{Co}(\text{CN})_6]$, which gives rise to a large value of the volume compressibility (small value of the bulk modulus). This factor alone gives rise to the existence of colossal values of the coefficients of thermal expansion, with the values of the Grüneisen parameters appearing to be normal. This work has pointed to the important role of Ag...Ag metallophilic interactions, although we cannot claim to have arrived at a complete understanding of how these give rise to such a shallow floor of the energy surface. More work is needed in this regard. Moreover, we have predicted that $\text{Au}_3[\text{Co}(\text{CN})_6]$ will show similar behaviour to $\text{Ag}_3[\text{Co}(\text{CN})_6]$, and we anticipate that other materials with metallophilic interactions will also display extreme behaviour such as colossal thermal expansion.

Acknowledgments

The authors would like to acknowledge useful discussions with Dr Dan Wilson (Frankfurt) and Prof David Keen (ISIS), and help from Dr Helen Chappell (Cambridge) in the use of visualisation tools. We thank Dr Victor Milman (Accelrys) for supplying the Co USP used in this work. The calculations were performed using the computational resources of CamGrid [14, 15].

References

- [1] Goodwin AL, Calleja M, Conterio MJ, Dove MT, Evans JSO, Keen DA, Peters L, Tucker MG. Colossal positive and negative thermal expansion in the framework material $\text{Ag}_3[\text{Co}(\text{CN})_6]$. *Science* **319**, 794–797 (2008)
- [2] Goodwin AL, Tucker MG, Keen DA, Dove MT, Peters L and Evans JSO. Argentophilicity-dependent colossal thermal expansion in extended Prussian Blue analogues. *Journal of the American Chemical Society*, submitted
- [3] Sleight AW. Isotropic negative thermal expansion *Annual Review of Materials Science* **28**, 29–43 (1998)
- [4] Mary TA, Evans JSO, Vogt T and Sleight AW. Negative thermal expansion from 0.3 to 1050 Kelvin in ZrW_2O_8 *Science* **272**, 90–92 (1996)
- [5] Hochella MF, Jr., Brown GE, Jr., Ross FK and Gibbs GV. High-temperature crystal chemistry of hydrous Mg-cordierites and Fe-cordierites. *American Mineralogist* **64**, 337–351 (1979)
- [6] Goodwin AL and Kepert CJ. Negative thermal expansion and low-frequency modes in cyanide-bridged framework materials. *Physical Review B* **71**, article number 140301 (2005)

- [7] Carpenter MA, Salje EKH, Graeme-Barber A, Wruck B, Dove MT and Knight KS. Calibration of excess thermodynamic properties and elastic constant variations associated with the alpha-beta phase transition in quartz. *American Mineralogist* **83**, 2–22 (1998)
- [8] Barron THK, Collins JG and White GK. Thermal expansion of solids at low temperatures. *Advances in Physics* **29**, 609–730 (1980)
- [9] Conterio MJ, Goodwin AL, Tucker MG, Keen DA, Dove MT, Peters L and Evans JSO. Local structure in $\text{Ag}_3[\text{Co}(\text{CN})_6]$: Colossal thermal expansion, rigid unit modes and argentophilic interactions. *Journal of Physics: Condensed Matter*, submitted
- [10] Segall MD, Lindan PJD, Probert MJ, Pickard CJ, Hasnip PJ, Clark SJ, Payne MC. First-principles simulation: ideas, illustrations and the castep code. *Journal of Physics: Condensed Matter* **14**, 2717–2743 (2002)
- [11] Page for GGA generated Potentials. <http://lorax.chem.upenn.edu/Research/psp-gga.html> (information retrieved February 2008)
- [12] Monkhorst HJ, Pack JD, Special points for brillouin-zone integrations. *Physical Review B* **13**, 5188–5192 (1976)
- [13] Pauling L and Pauling P. A tritriculate crystal structure: trihydrogen cobaltcyanide and trisilver cobaltcyanide. *Proceedings of the National Academy of Sciences of the United States of America* **60**, 362–367 (1968)
- [14] Calleja M, Beckles B, Keegan M, Hayes MA, Parker A and Dove MT. CamGrid: Experiences in constructing a university-wide, Condor-based grid at the University of Cambridge. *Proceedings of the UK e-Science All Hands Meeting 2004 (ISBN 1-904425-21-6)*, pp 173–178 (2004) (obtainable from <http://www.allhands.org.uk/2004/proceedings/papers/99.png>, February 2008)
- [15] Calleja M. A University of Cambridge computational grid. <http://www.escience.cam.ac.uk/projects/camgrid/> (information retrieved February 2008)
- [16] Thain D, Tannenbaum T, Livny M. Distributed Computing in Practice: The Condor Experience. *Concurrency and Computation: Practice and Experience* **17**, 323–356 (2005)
- [17] Squyres JM and Lumsdaine A. A Component Architecture for LAM/MPI. in *Proceedings of the 10th European PVM/MPI Users' Group Meeting, 2840*, pp 379–387 (2003)
- [18] Segall MD, Pickard CJ, Shah R and Payne MC. Population analysis in plane wave electronic structure calculations. *Molecular Physics* **89**, 571–577 (1996)
- [19] Segall MD, Shah R, Pickard CJ and Payne MC. Population analysis of plane wave electronic structure calculations of bulk materials. *Physical Review B* **54**, 16317–16320 (1996)
- [20] Pyykko P, Runeberg N, Mendizabal F. Theory of the $d(10)$ - $d(10)$ closed-shell attraction .1. Dimers near equilibrium. *Chemistry – A European Journal* **3**, 1451–1457 (1997)
- [21] Pyykko P. Relativity, gold, closed-shell interactions, and CsAu.NH_3 . *Angewandte Chemie – International Edition*. **41**, 3573–3578 (2002)
- [22] Pyykko P. Theoretical chemistry of gold. *Angewandte Chemie – International Edition*. **43**, 4412–4456 (2004)
- [23] Du AJ and Smith SC. Van der Waals-corrected density functional theory: benchmarking for hydrogennanotube and nanotubenanotube interactions. *Nanotechnology* **16**, 2118–2123 (2005)
- [24] The k-vector types and Brillouin zones of the space groups, http://www.cryst.ehu.es/cryst/get_kvec.html (information retrieved February 2008)
- [25] Haser R, de Broin CE and M. Pierrot. Etude structurale de la serie des hexacyanoferrates(II,III) d'hydrogene: $\text{H}_{3+x}[\text{Fe}_x^{\text{II}}\text{Fe}_{1-x}^{\text{III}}(\text{CN})_6].y\text{H}_2\text{O}$. I. Structures cristallines des phases hexagonales H, $\text{H}_3\text{Fe}^{\text{III}}(\text{CN})_6$ et $\text{H}_3\text{Co}^{\text{III}}(\text{CN})_6$, par diffraction des rayons X et des neutrons. *Acta Crystallographica B* **28**, 2530–2537 (1972)
- [26] Colis JCF, Laroche C, Staples R, Herbst-Irmer R, and Patterson H. Structural studies of lanthanide ion complexes of pure gold, pure silver and mixed metal (gold silver) dicyanides. *Dalton Transactions*, 675–679 (2005)
- [27] Dove MT. *Structure and dynamics: and atomic view of materials*, Oxford University Press (ISBN10: 0198506783, 360 pp) (2003)
- [28] Heine V, Welche PRL, Dove MT. Geometrical origin and theory of negative thermal expansion in framework structures. *Journal of the American Ceramic Society* **82**, 1793–1802 (1999)
- [29] Hammonds KD, Dove MT, Giddy AP, Heine V, Winkler B. Rigid-unit phonon modes and structural phase transitions in framework silicates. *American Mineralogist* **81**, 1057–1079 (1996)
- [30] Pryde AKA, Hammonds KD, Dove MT, Heine V, Gale JD, Warren MC. Origin of the negative thermal expansion in ZrW_2O_8 and ZrV_2O_7 . *J. Phys.: Condensed Matter* **8**, 10973–10982 (1996)